chemistry proceedings

MDPI

Proceeding Paper

Designing and In Silico Evaluation of Some Non-Nucleoside *MbtA* Inhibitors: On Track to Tackle Tuberculosis †

Gourav Rakshit and Venkatesan Jayaprakash *

Department of Pharmaceutical Sciences and Technology, Birla Institute of Technology, Mesra, Ranchi 835215, Jharkhand, India

* Correspondence: drvenkatesanj@gmail.com

† Presented at the 26th International Electronic Conference on Synthetic Organic Chemistry, 15–30 November 2022; Available online: https://sciforum.net/event/ecsoc-26.

Abstract: The WHO database shows that mycobacterium tuberculosis has become an epidemic worldwide due to its pathogenicity and virulence, which have magnified its infectiousness. The situation becomes grimmer with the prevalence of MDR-TB, XDR-TB, emergence of cross-resistance, ineffectiveness of novel therapeutic targets, failure of novel medications in clinical trials, currently available drugs losing their therapeutic efficacy, lack of drug discovery efforts due to poor ROI, and the existence of co-infections; i.e., HIV, TB, COVID, and HIV-TB-COVID. Following our prior studies described by Stirret et al. in 2008, Ferreras et al. in 2011, and Shyam et al. in 2021, herein we focus on exploring pyrazoline-based mycobactin analogs (non-specific mycobactin biosynthesis inhibitors) targeting the *MbtA* enzyme (first step of mycobactin biosynthesis) with a hope of finding a more potent analog showing a high affinity for *MbtA*. The design strategy involves retaining the structural features of mycobacterial siderophores. Herein, a small library (12 molecules) of mycobactin analogs were designed, keeping the necessary skeleton (diaryl-substituted pyrazoline (DAP)) intact and assessed their stability using in silico tools. In order to determine the binding modes and inhibitory profiles of the designed ligands, docking was carried out in the active pocket of *MbtA* (analogous with the homologous structure with PDB ID: 1MDB). The best energy conformation (lowest score) of each docked ligand was represented graphically. The ADMET profile of each molecule was analyzed. The best molecule that revealed a good ADMET profile was taken up for MD simulation study (45 ns). Results revealed that the designed compounds GV08 (−8.80 kcal/mol, 352.58 nM), GV09 (−8.61 kcal/mol, 499.91 nM), GV03 (−8.59 kcal/mol, 508.51 nM), and GV07 (−8.54 kcal/mol, 553.44 nM) had a good docking score and inhibition constant. Of these, GV08 showed a good ADME profile with all the major parameters lying in the acceptable ranges. They also showed the least toxicity with no hepatotoxicity and skin sensitization. MD simulation studies of GV08 also suggest that it was stable throughout the course of simulation. This could be justified by RMSD, RMSF, and H-bond plots. The future scope invalidates these findings through synthesis, characterization, and intracellular activity.

Keywords: antitubercular drug discovery; *MbtA*; molecular docking; MD simulation; mycobactin; siderophores; pyrazolines; non-nucleoside *MbtA* inhibitors

Citation: Rakshit, G.; Jayaprakash, V. Designing and In Silico Evaluation of Some Non-Nucleoside *MbtA* Inhibitors: On Track to Tackle Tuberculosis. *Chem. Proc.* **2022**, *12*, 78. https://doi.org/10.3390/ecsoc-26-13688

Academic Editor: Julio A. Seijas

Published: 17 November 2022

1. Background

Mycobacterium tuberculosis is the prime causative agent of the lethal disease tuberculosis. It is an airborne, infectious, and ultimately fatal bacillus that causes tuberculosis (Mtb) [1]. This disease has been plaguing humans for centuries and has recently become a major international health concern. To eradicate tuberculosis by the year 2030 is one of the prime health objectives of the UN Sustainable Development Goals (SDGs). The World Health Organization released its Global Tuberculosis Report on 14 October 2021, providing an in-depth look at the devastating effects of this illness [2]. In 2020, there were 5.8 million

new cases of infection reported worldwide, putting us right back where we were in 2012 [3]. Additionally, 1.5 million HIV-negative people died around the world. Reduced access to TB diagnosis and treatment, as well as a lack of drug discovery initiatives, are likely to blame for these concerning infection rates. The increasing prevalence of MDR-TB and XDR-TB, the emergence of cross-resistance, the fact that current targets were resistant to treatment, the ineffectiveness of novel therapeutic targets, and the failure of novel medications in clinical trials has prompted the development of novel chemotherapeutic treatments with improved efficacy over the currently available drugs [4]. The burden is further increased by the occurrence and emergence of co-infections with HIV, TB, COVID, and HIV-TB-COVID [5]. This emphasizes the necessity of employing novel chemical entities functioning through unique mechanisms to combat the growing threat of this infectious killer disease on a worldwide scale. The idea of "conditionally essential target" (CET)-based drug design can help with this. The identification and targeting of conditionally essential targets are a common focus in the development of effective chemotherapeutic treatments for infectious diseases (CET). To this end, we are applying a theory proposed by Prof. Luis E. N. Quadri, who hypothesized that concentrating on a conditionally necessary pathway in the host–pathogen machinery would aid in the discovery of new antibacterial drugs. One such CET that has been shown to be useful in the mycobacterial life cycle and replication is the mycobactin biosynthesis pathway (MBP) [6]. In response to iron-deficient conditions, mycobacteria up-regulate the MBP and begin to uptake mycobactins (siderophores/iron chelators). The mycobactin megasynthase cluster encodes a mixed non-ribosomal peptide synthetase–polyketide synthase (NRPS–PKS) system that is responsible for the synthesis of mycobactin (siderophore). This cluster consists of 14 conditionally essential genes (*mbtA*–mbtN). Salicyl-AMP ligase (*MbtA*) and phenyloxazoline synthase (MbtB) are two essential enzymes in this biosynthetic pathway. For this reason, it has been deemed a potentially fruitful endogenous target for the discovery of novel lead molecules/inhibitors. As a possible *MbtA* inhibitor, nucleoside analogues have been studied extensively since the turn of the millennium. Our lab at BIT Mesra is focusing on finding non-nucleosidic analogues instead, as these have poor pharmacokinetic profiles. Our objective is to generate non-nucleosidic analogues (pyrazoline-based mycobactin-mimicking compounds) by retaining the structural features of mycobacterial siderophores in the hope that they will inhibit the siderophores biosynthesis enzyme (*MbtA*), thereby stopping bacterial growth in iron-deficient environments. Herein, we aim to explore the SAR of the earlier reported potent molecules as described by Stirret et al. in 2008 [7], Ferreras et al. in 2011 [8], and Shyam et al. in 2021 [9]. In a quest to find novel compounds (non-nucleosidic analogues) having a high affinity for *MbtA*, we designed 12 molecules by retaining the diaryl-substituted pyrazoline (DAP) scaffold. The designed molecules are presented in Table 1. The putative compounds were docked in the *MbtA* receptor active site to determine their binding affinities and inhibitory profiles (analogous with the homologous structure with PDB ID: 1MDB). Top four docked ligand's lowest energy conformation (highest score) was displayed in a BIOVIA discovery studio [10]. The absorption, distribution, metabolism, excretion, and toxicity (ADMET) profile of the top four compounds was analyzed. Good ADMET profile molecules were selected for further MD simulation (45 ns).

Table 1. The list of 12 designed molecules.

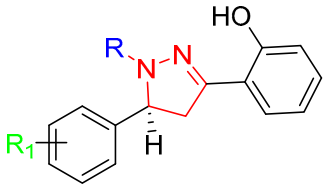

S. No.	Code	R	R_1
01	GV01	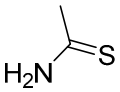	2-CH_3
02	GV02	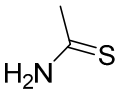	3-CH_3
03	GV03	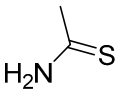	4-CH_3
04	GV04	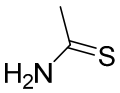	2-OCH_3
05	GV05	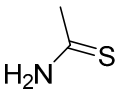	3-OCH_3
06	GV06	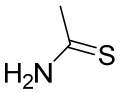	4-OCH_3
07	GV07	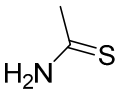	2-Cl
08	GV08	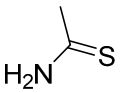	3-Cl
09	GV09	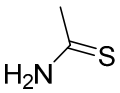	4-Cl
10	GV10	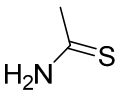	2-OH
11	GV11	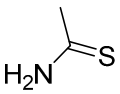	3-OH
12	GV12	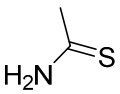	4-OH

2. Materials and Methods Employed

2.1. Hardwares and Softwares Used

All the in silico molecular docking studies were carried out using a workstation. The specifications were: (i) make: DELL; (ii) OS (64-bit): Ubuntu 20.04.3 LTS; (iii) processor: Intel® Core™ i7: 11-800 CPU with 2.30 GHz speed; (iv) RAM: 16 GB; (v) GPU:

4 GB; and (vi) SSD: 1 TB. Softwares employed were: (i) molecular docking: Autodock-4.2.6; (ii) sketching of ligands: ChemDraw 19.0 (Perkin-Elmer); (iii) visualizations: UCSF Chimera 1.13.1. [11] and BIOVIA Discovery Studio Visualizer; and (iv) molecular dynamics simulations (MDSs): GROMACS [12,13].

2.2. Molecular Docking Simulations

2.2.1. Preparation of Protein

The 3D X-ray crystal structure of salicyl-AMP ligase (*MbtA*) was utilized for this study. The PDB file was obtained from the Alpha Fold Protein Structure Database [14,15]. The protein preparation steps involved: (i) the txhe *.pdb* file was uploaded in the AutoDock program, (ii) water molecules were extracted, (iii) the addition of polar hydrogens, (iv) the addition of gasteiger charges, and the final structure was saved as *.pdbqt* format for docking [16].

2.2.2. Preparation of Ligands

The ligand preparation steps involved: (i) drawing the 2D structure of the respective ligand in ChemDraw 19.1, (ii) conversion of 2D to 3D using Chem3D 19.1, (iii) energy minimization using the MM_2 tool, and (iv) saving the final structure in *.pdb* format for docking.

2.2.3. Molecular Docking Studies

AutoDock 4.2.6, which employs a Lamarckian genetic algorithm, was used to perform molecular docking [16]. A grid box (binding site box) of dimensions 60 × 60 × 60 in the x, y, and z directions was built by centering on the nucleotide binding pocket (analogous with the homologous structure with PDB ID: 1MDB). Other parameters pertaining to docking were kept as default: (i) population size: 150; (ii) number of genetic algorithms runs: 50; and (iii) number of evaluations: 2500000. Auto grid-4.2. The map files were generated using Auto grid-4.2.6. Docking was run for each ligand using Auto dock-4.2.6. Results were sorted from the *.dlg* file based on the lowest energy structural conformation of each docked ligand. The 2D and 3D visualizations were conducted using the BIOVIA Discovery Studio Visualizer.

2.3. Predictive Absorption, Distribution, Metabolism, and Excretion (ADME)

The top four scoring molecules from docking studies were taken up for predictive ADME studies. SWISSADME: a web-server (https://www.swissadme.ch) by the Swiss Institute of Bioinformatics molecular modelling group was used to compute the ADME properties (accessed on 5 October 2022) [17]. Respective ligands were drawn in the Marvin JS portal http://swissadme.ch/index.php (accessed on 5 October 2022). The 2D structures were converted to SMILES, followed by which the server predicted ADME properties.

2.4. Prediction of Toxicity

Prediction of toxicity seems to be an essential property for all compounds. PkCSM: a web-server database that predicts the information related to toxicity [18].

2.5. Molecular Dynamics Simulations

GROMACS (Groningen machine for chemicals simulations) 2019 package was used to carry out molecular dynamics simulation (MDS) [19]. The top hit molecule, as evidenced by molecular docking and predictive ADMET studies, was selected for MDS studies. The topology files for ligand were generated from SwissParam (https://www.swissparam.ch/ (accessed on 5 October 2022)) [20]. The addition of the sodium and chloride ions neutralized the system's charge. Using the steepest descent strategy, the complex's energy was minimized (1000 ps; 50,000 steps). Following this, a 45ns (450,000 steps) molecular dynamics simulation was run for the corresponding protein–ligand complex. Xmgrace (http://plasma-gate.weizmann.ac.il/Grace/ (accessed on 5 October 2022)) was used to ex-

amine the root-mean-square deviation and fluctuation (RMSD/F), intramolecular hydrogen bonding, radius of gyration (ROG), and thermodynamic parameters.

3. Results and Discussions

3.1. Molecular Docking Simulations

Molecular docking simulation of the designed ligands was performed on the *MbtA* protein. All the ligands revealed favorable binding energies and inhibition constants. Of all the ligands, four displayed potential binding scores, namely: GV08 (−8.80 kcal/mol, 352.58 nM), GV09 (−8.61 kcal/mol, 499.91 nM), GV03 (−8.59 kcal/mol, 508.51 nM), and GV07 (−8.54 kcal/mol, 553.44 nM). They displayed strong negative binding energies and a strong affinity for the active binding pocket. Table 2 displays the detailed docking analysis (negative binding energy and inhibition constants) of all the designed ligands. Table 3 highlights the interacting residues and their interaction pattern (H-bond interactions). The 2D-interaction images highlighting the important residues are presented in Figures 1–4.

Table 2. Detailed docking score analysis of the ligands in the active pocket of *MbtA*.

S.No.	Coding	Docking Score (kcal/mol)	Inhibition Constant (K_i)
01	GV01	−8.19	996.73 nM
02	GV02	−8.53	563.3 nM
03	GV03	−8.59	508.51 nM
04	GV04	−8.26	878.26 nM
05	GV05	−7.97	1.45 µM
06	GV06	−7.88	1.67 µM
07	GV07	−8.54	553.44 nM
08	GV08	−8.80	352.58 nM
09	GV09	−8.61	499.91 nM
10	GV10	−7.96	1.47 µM
11	GV11	−7.88	1.67 µM
12	GV12	−7.70	2.29 µM

Table 3. Detailed docking interaction analysis of the top four ligands in the active pocket of *MbtA*.

S.No.	Coding	H-Bond Interacting Residues
1.	GV08	Glu357, Ala356, Thr462, Gly460
2.	GV09	Glu357, Ala356, Thr462, Gly460, Gly214
3.	GV03	Glu357, Ala356, Thr462, Gly460
4.	GV07	Gly330, Thr462, Gly460

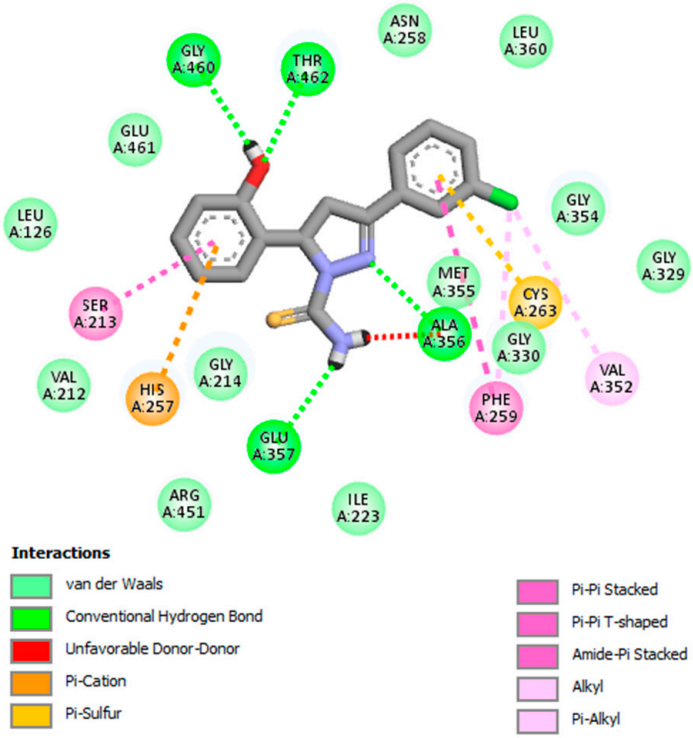

Figure 1. 2D-interaction image of GV08 showing various interacting residues and H bonds (four) in the active pocket of *MbtA*.

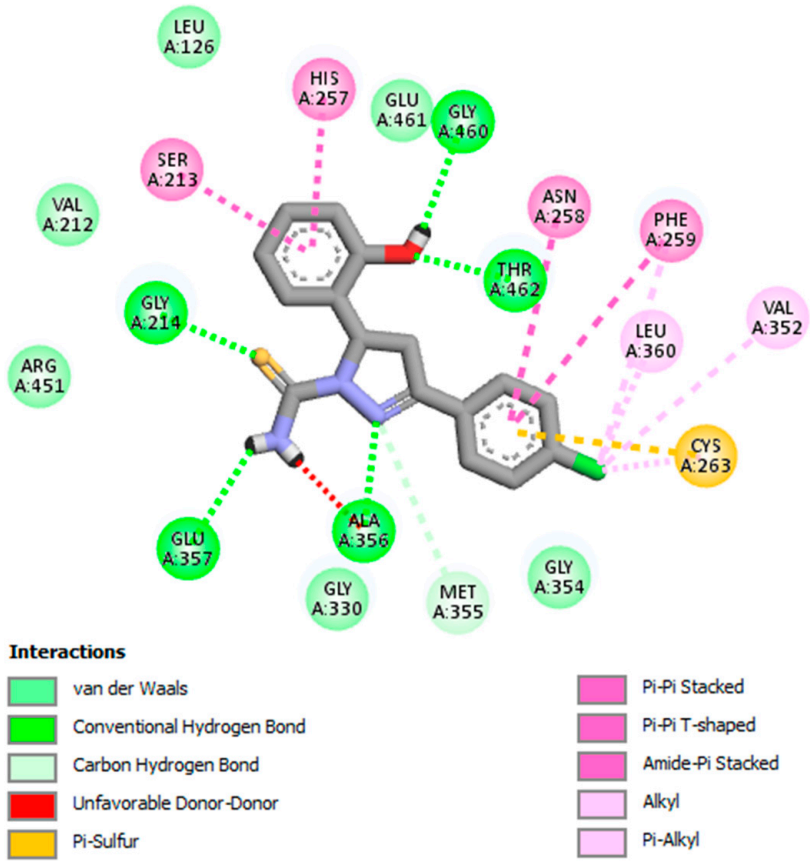

Figure 2. 2D-interaction image of GV09 showing various interacting residues and H bonds (five) in the active pocket of *MbtA*.

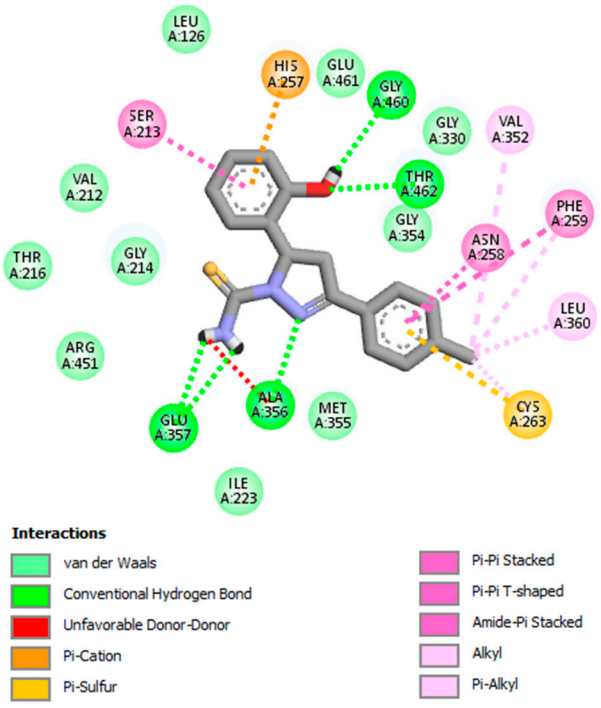

Figure 3. 2D-interaction image of GV03 showing various interacting residues and H bonds (four) in the active pocket of *MbtA*.

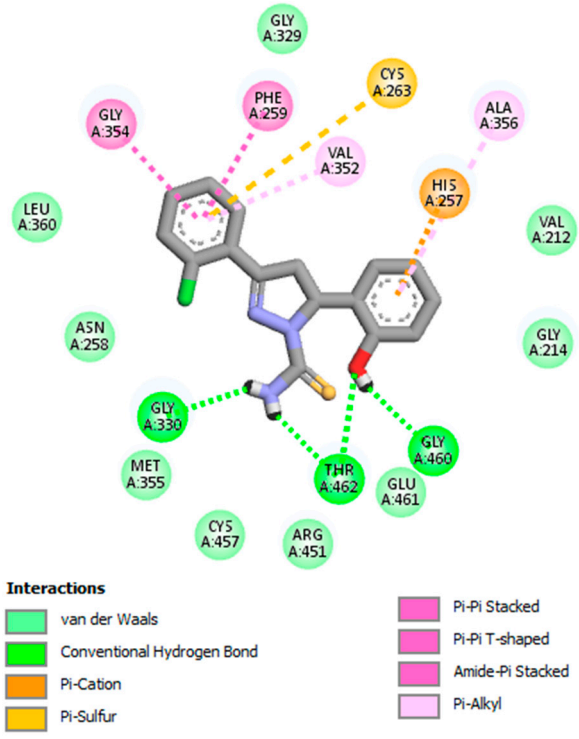

Figure 4. 2D-interaction image of GV07 showing various interacting residues and H bonds (three) in the active pocket of *MbtA*.

Interaction Analysis of GV08

GV08 revealed a higher binding energy (−8.80 kcal/mol, 352.58 nM). It made four hydrogen bonds with the active site amino acid residues, namely: Glu357, Ala356, Thr462, and Gly460. Glu357 helps in proton abstraction and donation. The binding of sub-

strate/inhibitor molecules at the active site induces small movements in the conformation of the protein, which is stabilized by the formation of H bonds. All the interactions with amino acid residues help in stabilization and orientation. The detailed interactions are presented in Figure 5.

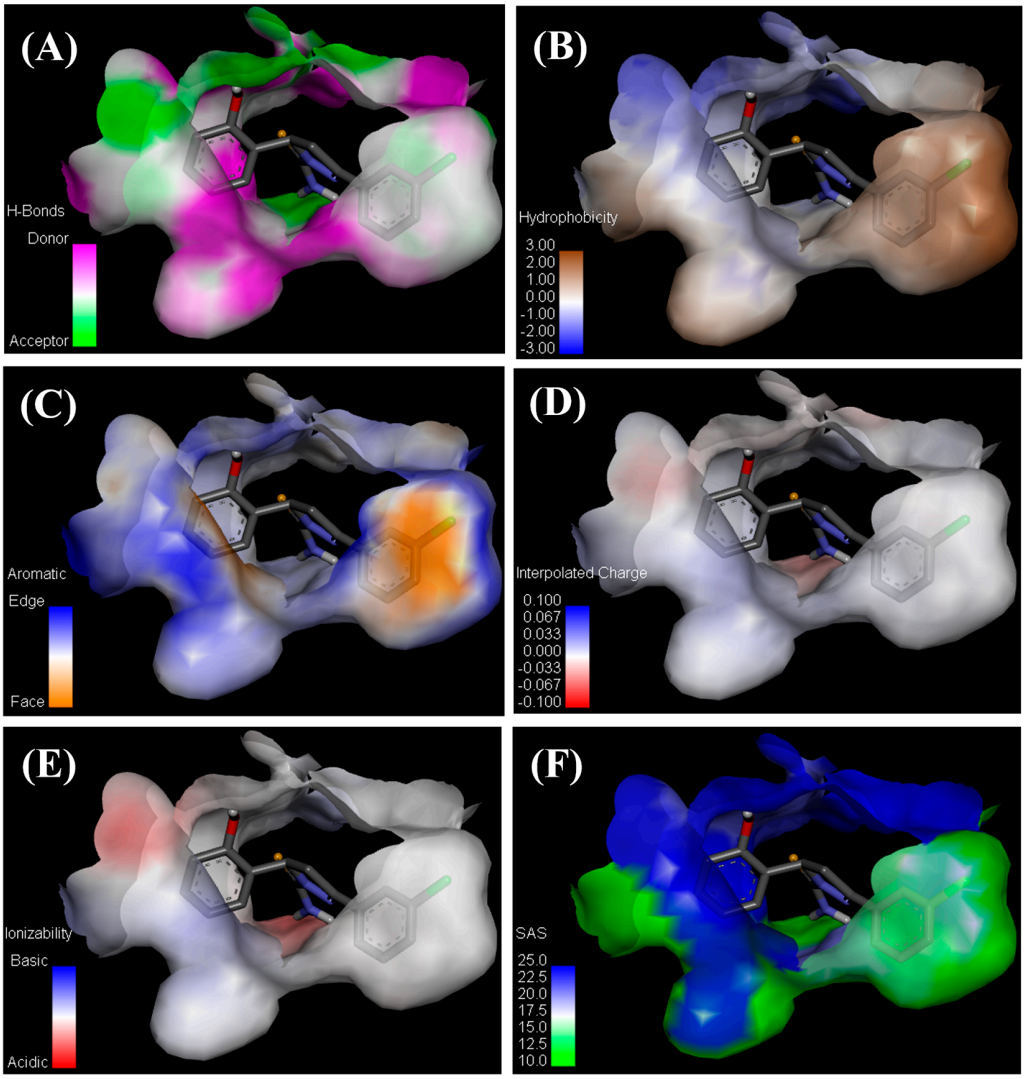

Figure 5. Various interactions of GV08 in the active-site pocket of *MbtA* stating how well the ligand fits in it; (**A**) H bonds, (**B**) hydrophobicity, (**C**) aromaticity, (**D**) charge distribution, (**E**) ionizability, and (**F**) solvent accessible surface area.

3.2. Predictive Absorption, Distribution, Metabolism, and Excretion (ADME)

3.2.1. Drug-Likeness, Alerts, Lead-Likeness, and Synthetic Accessibility

The word "drug-likeness" refers to a compound's propensity to bioavailability as an oral medication. Five different filters were used to determine the drug-likeness of our twelve query compounds, as shown in Table 4. All of the studied compounds (GV08, GV09, GV03, and GV07) exhibited outstanding drug-likeness scores, no breaches of drug-likeness regulations, and good lead-likeness scores, according to the data. The PAINS and Brenk algorithms were utilized to pinpoint the ambiguous sequences that may be responsible for spurious biological results. All the compounds were found to be in violation due to the presence of fragments. The compounds' lead-likeness was calculated in addition to their synthetic accessibility evaluation. The obtained information suggests that the four compounds with scores between 3.43 and 3.54 might be simple to synthesize. A

score of 11, 17, 56, or 85 on the Abbot bioavailability scale indicates that the molecule has a high probability of being orally bioavailable in rats and/or passing the Ca-co-2 cell line permeability assay, respectively. The expected bioavailability of all of the molecules was 56%.

Table 4. Various PAINS and Brenk drug-likeness rules, bioavailability data, lead-likeness metrics, synthetic access, and warnings are tabulated for easy perusal and comparison.

Sl No.	Compound Code	Drug-Likeness Rules						Alerts		Lead-Likeness	Synthetic Accessibility
		Lipinski (Pfizer)	Ghose (Amgen)	Veber (GSK)	Egan (Pharmacia)	Muege (Bayer)	Bioavailability Score	PAINS	Brenk		
1.	**GV08**	Yes	Yes	Yes	Yes	Yes	0.55	1	1	Yes	3.43
2.	**GV09**	Yes	Yes	Yes	Yes	Yes	0.55	1	1	Yes	3.43
3.	**GV03**	Yes	Yes	Yes	Yes	Yes	0.55	1	1	Yes	3.54
4.	**GV07**	Yes	Yes	Yes	Yes	Yes	0.55	1	1	Yes	3.51

3.2.2. Analysis of Pharmacokinetics Compliance through In Silico Evaluation

ADME is used to evaluate how well a substance is able to traverse the body (absorption, distribution, metabolism, and elimination). The ADME parameters for the compounds GV08, GV09, GV03, and GV07 were calculated by taking into account their specific chemical and biopharmaceutical properties. The molar refractivity refers to the overall polarity of the molecules. GV08, GV09, and GV07 have a molar refractivity of 99.56, while GV03 had 99.51. The acceptable range is 30–140. TPSA (topological polar surface area) was 93.94 $Å^2$ for all the molecules. These results show that the molecules are unable to cross the blood−brain barrier (BBB). Solubility class lipophilicity refers to a molecule's ability to dissolve itself in a lipophilic medium. The iLOGP values of all four molecules were in the acceptable range (GV08: 2.43; GV09: 2.41; GV03: 2.40; and GV07: 2.14) of −0.4 to +5.6. The SILICOS-IT results were quite promising (GV08: 3.90; GV09: 3.90; GV03: 3.77; and GV07: 3.90). The intestinal absorption of these substances was very high. A chemical's ability to dissolve in water is crucial to how well it will be absorbed and distributed in the body. The solubility in water at 25 °C is shown by its log S value. If one wishes to ensure proper solubility, the ESOL model's calculated log S values shouldn't be higher than 6. GV08, GV09, and GV07 all had a log S value of −3.99, while GM03's value was −3.70, indicating good solubility. The results indicate that these compounds have an appropriate balance of permeability and solubility; and hence, bioavailable when administered orally. The expected gastrointestinal (GI) absorption was high across the board. ADMET and cell-based bioassay data can be better understood with the help of permeability predictions. GV08, GV09, and GV07 all had permeabilities over human skin of 6.19 cm/s, whereas GV03's permeability was 6.25 cm/s, well within the allowable range. There was no evidence that any of these chemicals could breach through the BBB, as was previously mentioned. Problems with drug absorption and drug interactions may arise from metabolic factors. The free drug is the only form that can be bound by the enzymes that break it down. Understanding the metabolic behavior of our primary substances requires knowledge of their interaction with cytochrome P450 enzymes (CYPs), the most well-known class of metabolizing enzymes. The capacity to inhibit CYPs was evaluated for all four substances with only slight variations. Table 5 includes a discussion of the analyses performed.

Table 5. Detailed discussion of the ADME analyses performed for the four top hit compounds.

			GV08	GV09	GV03	GV07
ADMET PROFILING	Physiochemical parameters	Formula	$C_{16}H_{14}ClN_3OS$	$C_{16}H_{14}ClN_3OS$	$C_{17}H_{17}N_3OS$	$C_{16}H_{14}ClN_3OS$
		Molecular weight	331.82 g/mol	331.82 g/mol	311.40 g/mol	331.82 g/mol
		Mol. refractivity	99.56	99.56	99.51	99.56
		TPSA	93.94 Å^2	93.94 Å^2	93.94 Å^2	93.94 Å^2
	Lipophilicity	ILOGP	2.43	2.41	2.40	2.14
		SILICOS-IT	3.90	3.90	3.77	3.90
	Water solubility	Log S (ESOL), class	−3.99 Soluble	−3.99 Soluble	−3.70 Soluble	−3.99 Soluble
		Log S (Ali), class	−4.64 Moderately soluble	−4.64 Moderately soluble	−4.37 Moderately soluble	−4.64 Moderately soluble
		SILICOS-IT, class	−4.69 Moderately soluble	−4.69 Moderately soluble	−4.47 Moderately soluble	−4.69 Moderately soluble
	Pharmacokinetics	GI absorption	High	High	High	High
		BBB permeant	No	No	No	No
		Log K_p (skin perm.)	−6.19 cm/s	−6.19 cm/s	−6.25 cm/s	−6.19 cm/s
		CYP1A2	Yes	Yes	No	Yes
		CYP2C19	Yes	Yes	Yes	Yes
		CYP2C9	Yes	Yes	Yes	Yes
		CYP2D6	No	No	No	No
		CYP3A4	No	No	No	No

3.3. Prediction of Toxicity

The molecules GV08, GV09, GV03, and GV07 were investigated computationally for their potential toxicity. All of the molecules were determined to have a maximum tolerated dosage (human) between 0.053 and 0.101 log mg/kg/day. However, neither hERGI nor hERG II (human ether-a-go-go-related gene) inhibition was detected. Phospholipid accumulation within cells was not found in this study (known to cause QT prolongation, myopathy, hepatotoxicity reaction, nephrotoxicity, and pulmonary dysfunction). Only GV03 was projected to be hepatotoxic by the algorithms, and none of the chemicals were expected to cause cutaneous hypersensitivity. Table 6 lists all the projected toxicity data for molecules with the IDs GV08, GV09, GV03, and GV07.

3.4. Molecular Dynamics Simulations

The stability of ligand binding in the intended target's active site was investigated using molecular dynamics simulations for GV08−*MbtA*. In order to better understand the structure of macromolecules and how drug resistance occurs, several drug discovery applications employ MD research. We discuss the results of our simulations below. Significant RMSD values of 0.45 were found between the conformations of the *MbtA* protein, showing that the protein−ligand combination was kept in a static state throughout the simulation. The variation in structural confirmations over time can be understood via the lens of RMSD. RMSD values for the protein (0.45) and ligand (7.5) are displayed in Figure 6.

Table 6. Detailed discussion of the toxicity analyses performed for the four top hit compounds.

Name of Model	Unit	GV08	GV09	GV03	GV07
AMES toxicity	**Yes/No**	**No**	**No**	**No**	**No**
Max. tolerated dose (human)	**Log mg/kg/day**	0.053	0.085	0.101	0.087
hERG I inhibitor	**Yes/No**	No	No	No	No
hERG II inhibitor	**Yes/No**	No	No	No	No
Oral rat chronic toxicity (LD50)	**Mol/kg**	2.47	2.46	2.393	2.461
Oral rat chronic toxicity	**Log mg/kg_bw/day**	1.115	1.167	1.313	1.096
Hepatotoxicity	**Yes/No**	No	No	Yes	No
Skin sensitization	**Yes/No**	No	No	No	No
T. Pyriformis toxicity	**Log ug/L**	2.113	2.1	2.037	2.127
Minnow toxicity	**Log mM**	0.629	0.882	1.1	0.893

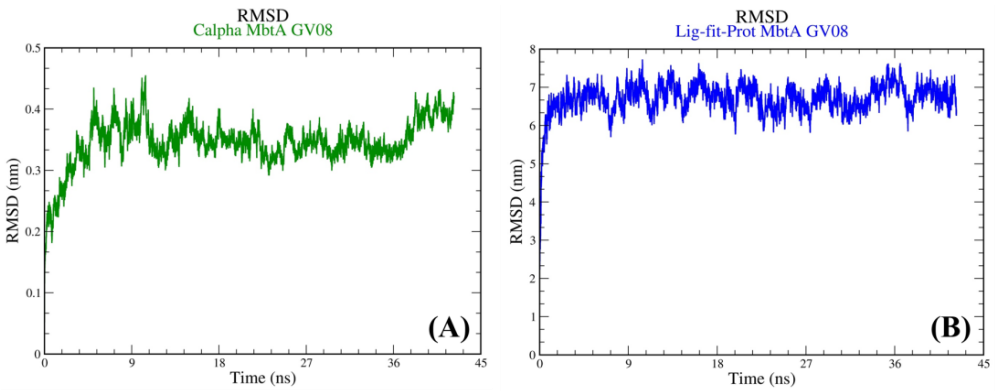

Figure 6. Protein RMSD (**A**) and ligand RMSD (**B**) of the *MbtA*−ligand complex formed by the compound with the lowest binding energy, GV08.

The average variation of a particle (such as a protein residue) over time from a reference position is measured by the root-mean-square fluctuation (RMSF) (typically the time-averaged position of the particle). As a result, RMSF examines the structural elements that deviate the most from their mean structure (or least). Herein, the protein fluctuated the least during the course of simulation; however, there were minor fluctuations in the ligand. These minor fluctuations are acceptable for small biomolecules (Figure 7). These RMSF values suggest the protein−ligand complex's stability.

The stability of the protein–ligand (*MbtA*−GV08) complex can be justified by various other parameters, which suggests the ligand's (GV08) ability to bind effectively to the active site pocket. Figures 8–10 highlights the various parameters associated with the protein−ligand complex during the course of simulation.

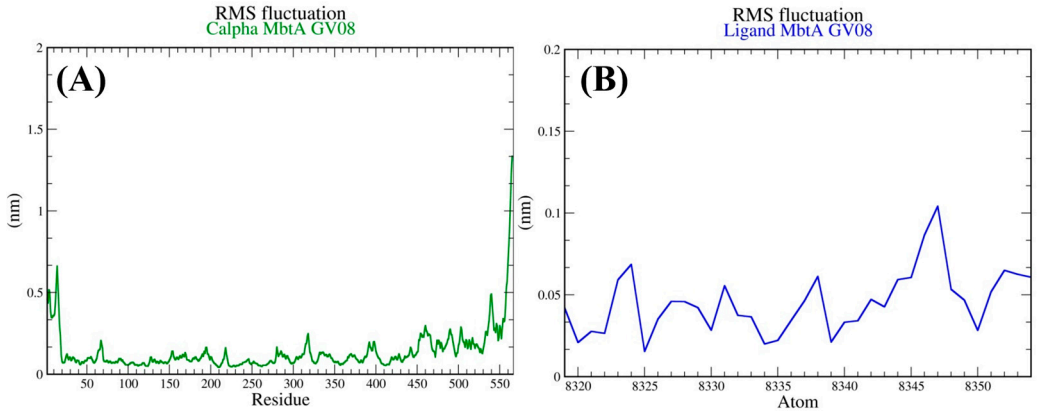

Figure 7. Root-mean-square fluctuation (RMSF) of the protein–ligand complex of *MbtA* with the lowest binding energy compound GV08; (**A**) RMSF of protein and (**B**) RMSF of ligand.

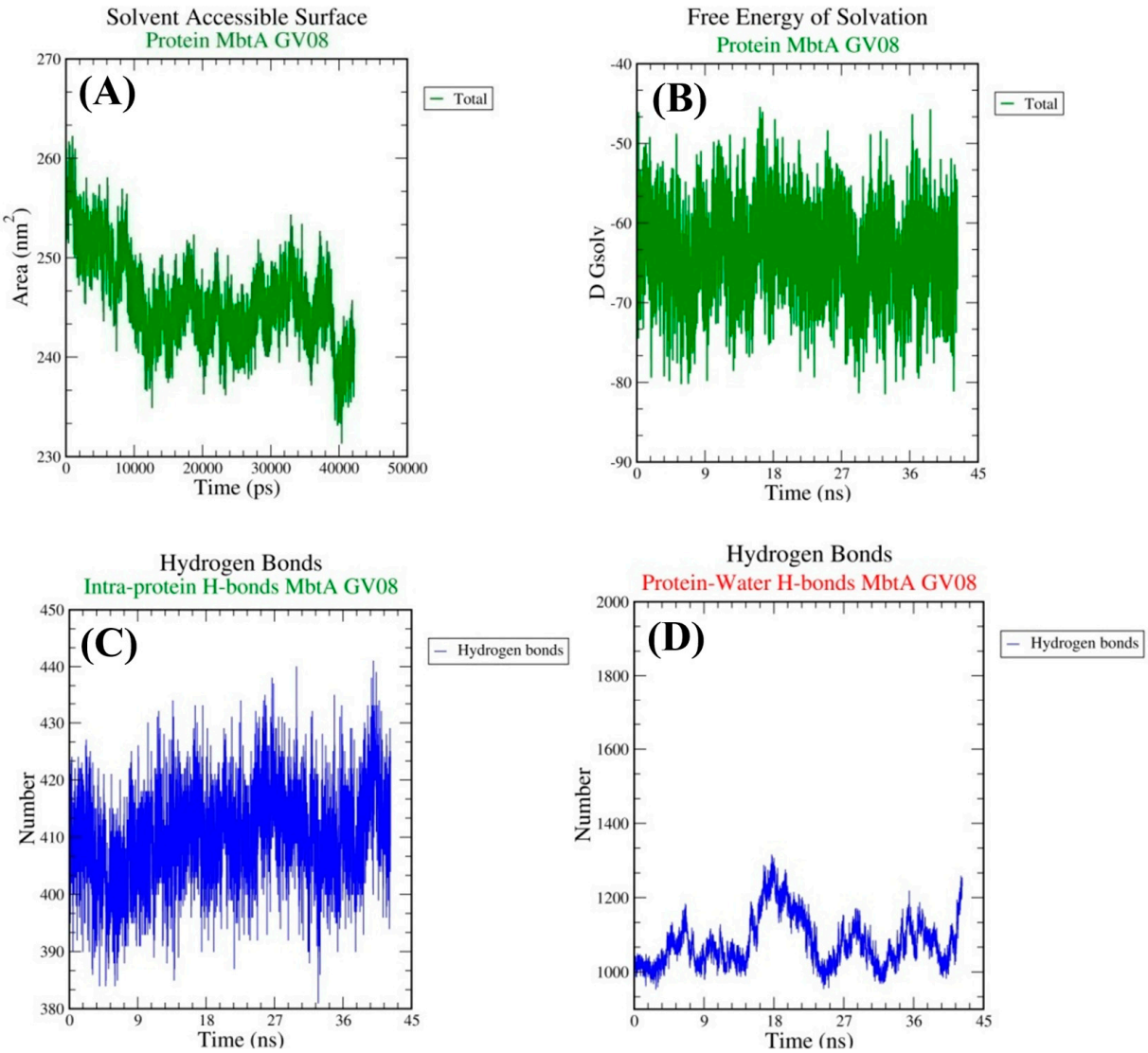

Figure 8. Various parameters of the protein–ligand complex of *MbtA* with the lowest binding energy compound GV08; (**A**) solvent accessible surface area, (**B**) free energy of solvation, (**C**) intra-protein hydrogen bonding, and (**D**) protein−water hydrogen bonding.

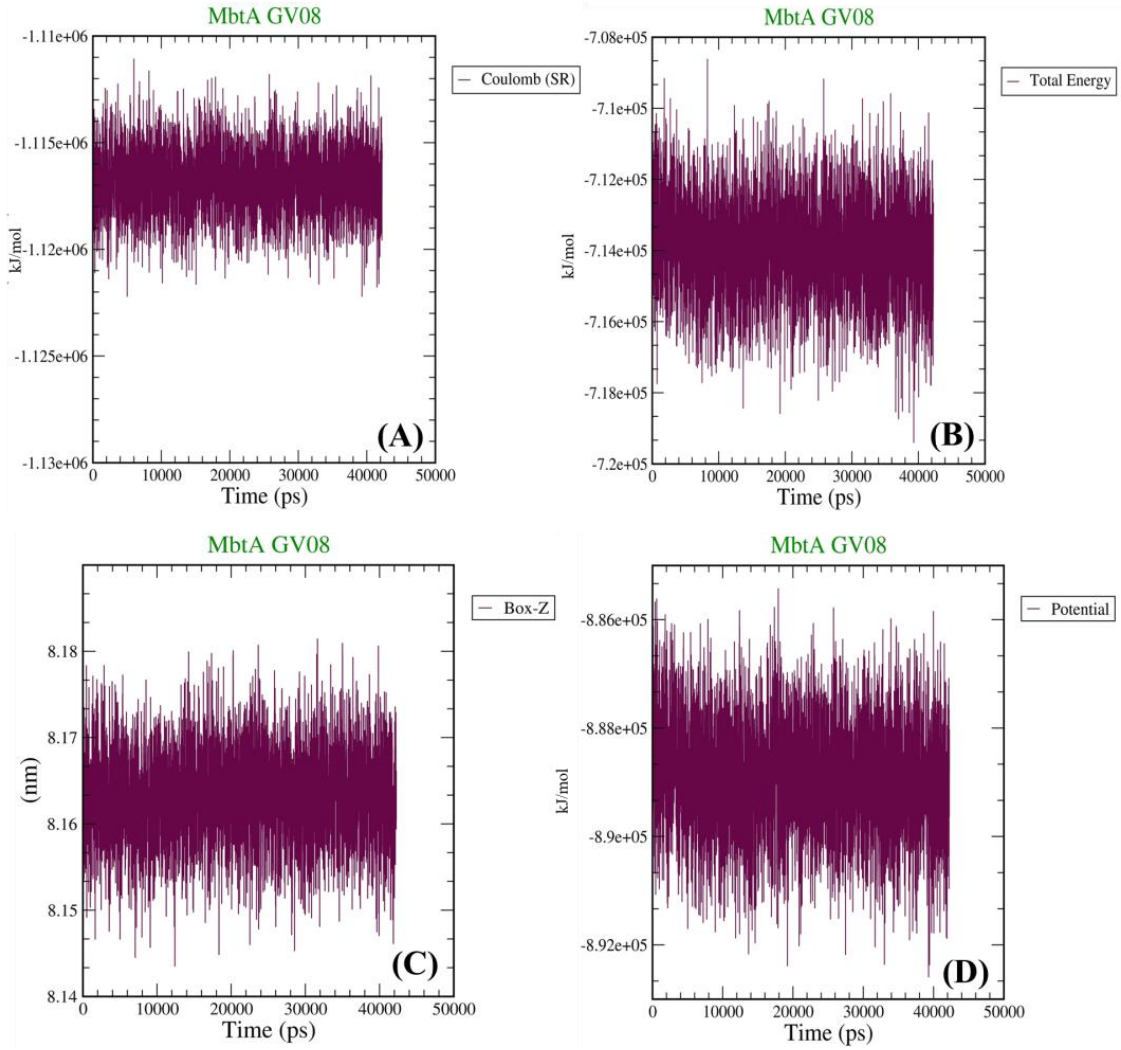

Figure 9. Various thermodynamics parameters of the protein–ligand complex of *MbtA* with the lowest binding energy compound GV08 highlighting the stability; (**A**) potential energy, (**B**) temperature, (**C**) density, and (**D**) total energy.

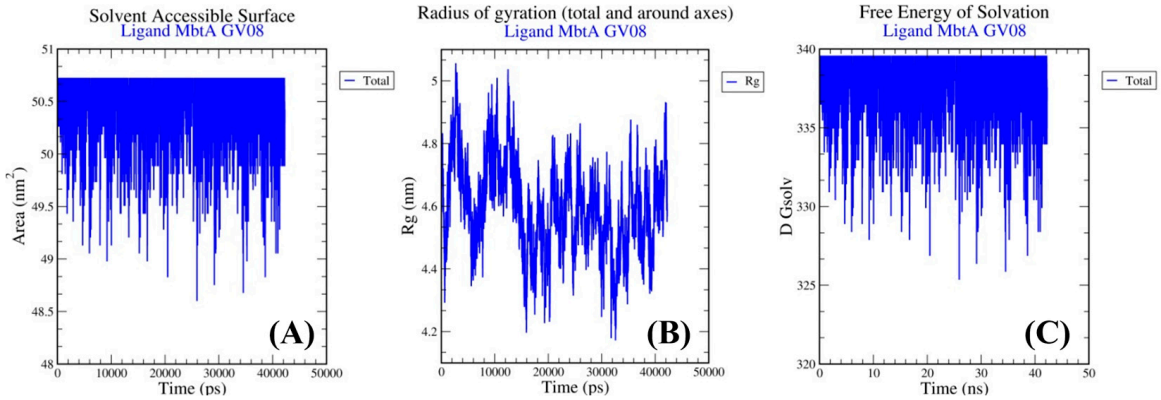

Figure 10. Various thermodynamics parameters of the protein–ligand complex of *MbtA* with the lowest binding energy compound GV08 highlighting the stability; (**A**) Solvent Accessible Surface Area, (**B**) Radius of Gyration, and (**C**) Free Energy of Solvation.

4. Conclusions

Despite tremendous advancements in the clinical drug candidate development for TB therapy during the past 10 to 15 years, TB remains a serious health burden in developing countries. Science is still focused on finding treatment possibilities that block novel targets. New treatment targets have been found as a result of research aimed at better understanding the biology of Mtb. It has been proven that imbalances in mycobactin synthesis and iron uptake have a direct impact on mycobacterial virulence and survival in the host. Structure-based rational design of MbtI and *MbtA* inhibitors has so far produced intriguing outcomes. In order to do this, we searched for M. tuberculosis inhibitors that can bind to a specific target, namely *MbtA*, using the concept of CET-based drug design. Our top four identified compounds (GV08, GV09, GV03, and GV07) were found to have strong interactions with the tubercular enzyme *MbtA*, a newly identified TB target that catalyzes the initial two-step process of mycobactin synthesis. Additionally, they displayed a minimal toxicity profile and a decent pharmacokinetic profile. GV08 was found to be the best molecule considering all the above parameters (predicted binding energy and pharmacokinetic profile). The stability of the complex (*MbtA*−GV08) was evaluated using MD simulation, the results of which revealed good stability. Based on these results, it could be concluded that GV08 could serve as a good lead for future optimization. The future scope lies in validating these findings by performing biological assays. Additionally, looking into the fundamental relationships between possible medications and their therapeutic uses may pave the way for the creation and application of novel and cutting-edge approaches for discovering new antibiotics.

Author Contributions: Conceptualization, V.J. and G.R.; methodology, G.R.; software, G.R.; validation, G.R.; formal analysis, G.R.; investigation, G.R.; resources, G.R.; data curation, G.R.; writing—original draft preparation, G.R.; writing—review and editing, G.R. and V.J.; visualization, G.R.; supervision, V.J.; project administration, V.J.; funding acquisition, V.J. and G.R. All authors have read and agreed to the published version of the manuscript.

Funding: Gourav Rakshit is thankful to the Birla Institute of Technology, Mesra, Ranchi for providing funding in the form of an Institute Research Fellowship Dean (PGS)/Ph.D/IRF/2021-2022/73 dated March 2021.

Institutional Review Board Statement: Not applicable.

Informed Consent Statement: Not applicable.

Data Availability Statement: Not applicable.

Acknowledgments: We would like to express our sincere gratitude to our Department of Pharmaceutical Sciences and Technology, Birla Institute of Technology, Mesra, Ranchi for providing the necessary software and supporting this research work. All individuals included in this study have consented to the acknowledgement.

Conflicts of Interest: The authors declare no conflict of interest.

References

1. Loddenkemper, R.; Murray, J.F.; Gradmann, C.; Hopewell, P.C.; Kato-Maeda, M. History of tuberculosis. *Tuberculosis* **2018**, 8–27. [CrossRef]
2. World Health Organization. *Global Tuberculosis Report*; WHO: Geneva, Switzerland, 2021.
3. World Health Organization. Tuberculosis. 2022. Available online: https://www.who.int/health-topics/tuberculosis#tab=tab_1 (accessed on 17 February 2022).
4. Nakajima, H. Tuberculosis: A global emergency. *World Health* **1993**, *46*, 3.
5. Bruchfeld, J.; Correia-Neves, M.; Källenius, G. Tuberculosis and HIV Coinfection: Table 1. *Cold Spring Harb. Perspect. Med.* **2015**, *5*, a017871. [CrossRef] [PubMed]
6. Shyam, M.; Shilkar, D.; Verma, H.; Dev, A.; Sinha, B.N.; Brucoli, F.; Bhakta, S.; Jayaprakash, V. The Mycobactin Biosynthesis Pathway: A Prospective Therapeutic Target in the Battle against Tuberculosis. *J. Med. Chem.* **2020**, *64*, 71–100. [CrossRef]

7. Stirrett, K.L.; Ferreras, J.; Jayaprakash, V.; Sinha, B.N.; Ren, T.; Quadri, L.E. Small molecules with structural similarities to siderophores as novel antimicrobials against Mycobacterium tuberculosis and Yersinia pestis. *Bioorg. Med. Chem. Lett.* **2008**, *18*, 2662–2668. [CrossRef] [PubMed]
8. Ferreras, J.A.; Gupta, A.; Amin, N.D.; Basu, A.; Sinha, B.N.; Worgall, S.; Jayaprakash, V.; Quadri, L.E.N. Chemical scaffolds with structural similarities to siderophores of non-ribosomal peptide–polyketide origin as novel antimicrobials against *Mycobacterium tuberculosis* and *Yersinia pestis*. *Bioorg. Med. Chem. Lett.* **2011**, *21*, 6533–6537. [CrossRef] [PubMed]
9. Shyam, M.; Verma, H.; Bhattacharje, G.; Mukherjee, P.; Singh, S.; Kamilya, S.; Jalani, P.; Das, S.; Dasgupta, A.; Mondal, A.; et al. Mycobactin Analogues with Excellent Pharmacokinetic Profile Demonstrate Potent Antitubercular Specific Activity and Exceptional Efflux Pump Inhibition. *J. Med. Chem.* **2022**, *65*, 234–256. [CrossRef]
10. Dassault Systèmes. *BIOVIA Discovery Studio Visualizer*; V16.1.0.15350; Dassault Systèmes: San Diego, CA, USA, 2016.
11. Pettersen, E.F.; Goddard, T.D.; Huang, C.C.; Couch, G.S.; Greenblatt, D.M.; Meng, E.C.; Ferrin, T.E. UCSF Chimera-a visualization system for exploratory research and analysis. *J. Comput. Chem.* **2004**, *25*, 1605–1612. [CrossRef]
12. Bjelkmar, P.; Larsson, P.; Cuendet, M.A.; Hess, B.; Lindahl, E. Implementation of the CHARMM Force Field in GROMACS: Analysis of Protein Stability Effects from Correction Maps, Virtual Interaction Sites, and Water Models. *J. Chem. Theory Comput.* **2010**, *6*, 459–466. [CrossRef] [PubMed]
13. Abraham, M.J.; Murtola, T.; Schulz, R.; Páll, S.; Smith, J.C.; Hess, B.; Lindahl, E. GROMACS: High performance molecular simulations through multi-level parallelism from laptops to supercomputers. *SoftwareX* **2015**, *1–2*, 19–25. [CrossRef]
14. Varadi, M.; Anyango, S.; Deshpande, M.; Nair, S.; Natassia, C.; Yordanova, G.; Yuan, D.; Stroe, O.; Wood, G.; Laydon, A.; et al. AlphaFold Protein Structure Database: Massively expanding the structural coverage of protein-sequence space with high-accuracy models. *Nucleic Acids Res.* **2022**, *50*, D439–D444. [CrossRef] [PubMed]
15. Berman, H.M.; Westbrook, J.; Feng, Z.; Gilliland, G.; Bhat, T.N.; Weissig, H.; Shindyalov, I.N.; Bourne, P.E. The Protein Data Bank. *Nucleic Acids Res.* **2000**, *28*, 235–242. [CrossRef] [PubMed]
16. Rizvi, S.M.D.; Shakil, S.; Haneef, M. A simple click by click protocol to perform docking: Autodock 4.2 made easy for non-bioinformaticians. *EXCLI J.* **2013**, *12*, 830–857.
17. Daina, A.; Michielin, O.; Zoete, V. SwissADME: A free web tool to evaluate pharmacokinetics, drug-likeness and medicinal chemistry friendliness of small molecules. *Sci. Rep.* **2017**, *7*, 1–13. [CrossRef] [PubMed]
18. Pires, D.E.V.; Blundell, T.L.; Ascher, D.B. pkCSM: Predicting Small-Molecule Pharmacokinetic and Toxicity Properties Using Graph-Based Signatures. *J. Med. Chem.* **2015**, *58*, 4066–4072. [CrossRef]
19. Pronk, S.; Páll, S.; Schulz, R.; Larsson, P.; Bjelkmar, P.; Apostolov, R.; Shirts, M.R.; Smith, J.C.; Kasson, P.M.; Van Der Spoel, D.; et al. GROMACS 4.5: A high-throughput and highly parallel open-source molecular simulation toolkit. *Bioinformatics* **2013**, *29*, 845–854. [CrossRef]
20. Zoete, V.; Cuendet, M.A.; Grosdidier, A.; Michielin, O. SwissParam: A fast force field generation tool for small organic molecules. *J. Comput. Chem.* **2011**, *32*, 2359–2368. [CrossRef]